Contents lists available at SciVerse ScienceDirect

Powder Technology

Preparation and characterization of nanocrystalline titania powders by sonochemical synthesis

Özlem Çağlar Duvarci *, Muhsin Çiftçioğlu

Chemical Engineering Department, Izmir Institute of Technology, Urla, IZMIR, Turkey

ABSTRACT

Nanocrystalline mesoporous titania powders were synthesized by hydrolyzing titanium isopropoxide in ethanol–water mixtures which were ultrasonically treated without using any templates or chemicals. Titanium isopropoxide–ethanol mixture was added dropwise to a water–ethanol mixture placed in an ultrasonic bath. The properties of the sonochemically synthesized powder were compared with those of the powders prepared without ultrasonic treatment along with Degussa P-25 titania powder. The phase structure, crystallite size, surface area, particle size, powder density were determined and sintering behavior was analyzed in this work. The nanotitania powder prepared during ultrasonic induced hydrolysis (TiO$_2$-U) was determined to be formed from a mixture of anatase and brookite phases at 25 °C. The brookite phase in nanotitania powder prepared without ultrasonic treatment (TiO$_2$-NoU) was detected at 70 °C. The anatase–rutile phase transformation was completed in the 500–700 °C range for both powders. The average crystallite sizes of the powders at 25 °C were determined as 10 and 5 nm for TiO$_2$-NoU and TiO$_2$-U, respectively. The surface area decreased from 238 to 106 m^2/g for TiO$_2$-NoU and from 287 to 82 m^2/g for TiO$_2$-U when the calcination temperature was increased from 200 to 500 °C. The evolution of the N$_2$ adsorption–desorption behavior with calcination temperature and the corresponding pore size distributions/volumes was attributed to the formation of closely packed submicron aggregates during powder synthesis and calcination. The sintering behavior was concluded to be controlled by 7–10 nm crystallites and the submicron aggregates. The determination of the densification behavior of titania powders prepared by different methods with various levels of dopants may prove to be very useful for a better understanding of the phase/pore structure evolution which is crucial for a significant number of applications.

© 2012 Elsevier B.V. All rights reserved.

1. Introduction

The emergence of nanomaterials had a great impact on several domains of science and technology such as chemistry, electronics, biotechnology, etc. Numerous applications based on optical, electrical, magnetic, catalytic, biological, or mechanical properties of nanomaterials originate from their unique and finely tunable nanostructures which make their synthesis one of the most promising and challenging research and development areas.

Establishing the relations between performance of the final product and the properties of the precursors and powders, their processing conditions, and the production rates necessitates a delicate continuous effort. The large scale production of starting precursors and nanomaterials with desired properties may accelerate the realization of the potential applications especially towards the supply of novel solutions to the cumulative need for sustainable clean energy and environmental pollution problems facing mankind.

Nanopowders/nanomaterials with novel physical, chemical, and mechanical properties can be utilized as the main building blocks of innovative solutions to the problems in energy, environment, health, communication and related areas. The functionality of a nanomaterial may rely on the surface area to volume ratio because the interactions with the surrounding media strongly depend on the extent of the surface area and the nature of the material surface.

Nanotitania gained considerable attention due to its potential and current uses such as ceramics [1], hydrogen [2] and carbon monoxide [3] gas sensors, catalytic and photocatalytic applications [4–7] including medicine, environmental cleaning [8,9], disinfection [10,11], hydrogen production from water [12], artificial photosynthesis [13,14] and thin film applications for solar cells and self-cleaning/antibacterial/hydrophilic surfaces [15].

Preparation methods and conditions have a great influence on the properties of titania powders such as size, shape, phase/pore structure, surface properties and phase transformations [16]. High surface area nanoparticles have been produced via ultrasonic irradiation in which the shock waves are capable of rupturing chemical bonds, generating highly reactive chemical species, and increasing mass transfer with particular effects on nucleation/crystal growth during powder preparation. The chemical effects of ultrasonic irradiation are based on acoustic

* Corresponding author.
E-mail addresses: ozlemduvarci@iyte.edu.tr (Ö.Ç. Duvarci),
muhsinciftcioglu@iyte.edu.tr (M. Çiftçioğlu).

cavitation where micro cavities in liquid medium form, grow, and collapse violently in extremely short time periods. The implosive collapse of cavities generates localized regions with high temperatures (~5000 K) and pressures (~1000 atm) at high heating/cooling rates (>10^{10} K/s) which are called hot spots [17–20]. The cavities (bubbles) contain vapor generated from either the liquid medium or the dissolved volatile gas/reagents. The vapor is subjected to high temperatures and pressures on collapse of the bubbles and results in molecular fragmentation with generation of highly reactive chemical species. These species might be H•, OH• and even H_2O_2 for water. The evolution of the bubbles causes impingements on the surfaces producing erosion at and around the point of impact, causes the removal of particles from the surface and disorganizes the surface thus creating local defects, dislocations, and vacancies at the solid–liquid interface [21].

Ultrasonic irradiation can be applied during or after precipitation of titanium salt/alkoxide precursors in water or ethanol–water mixtures. Investigations on the application of ultrasonic treatment after precursor mixing have shown that secondary phase formation and crystallite size of the powders were dependent on the ethanol–water ratio and duration of ultrasonic irradiation [22–24]. It was reported that the brookite phase formation ceased and the nature of the precipitates were no longer amorphous with decreasing ethanol–water ratio. The prolonged ultrasonic irradiation time was also observed to reduce the crystallite size of titania powders in the above studies.

The addition of precursor (titanium isopropoxide—TIP or titanium tetrachloride—TTC) into water or ethanol–water mixture by injection was also investigated [25]. The temperature of the mixture reached 100 °C when ultrasonic treatment was terminated. The final phases of the powders were determined as being amorphous, anatase, rutile, anatase–rutile or brookite–anatase mixture depending on the precursor composition. The N_2 sorption isotherms displayed H2 and H3 hysteresis loops indicating that the powders were mesoporous. The largest surface area (290 m²/g) was obtained from the powder which was recovered from the supernatant of hydrolyzed TIP after centrifugation. The phase structure was reported to depend on precursor composition (TIP/TTC) and reaction temperature. These findings were further explained to be due to the formation of a larger number of seed nuclei in the gel when the precursor was pure TIP.

The dropwise addition of titanium butoxide into water under ultrasonic irradiation caused the formation of micro/mesoporous titania powders [26]. Ultrasonic irradiation led to the formation of a crystalline powder (anatase and brookite mixture), while the powder without ultrasonic treatment was amorphous. The surface area and pore diameter of the powder prepared under ultrasonic irradiation after heat treatment at 100 °C were 264 m²/g and 4.3 nm respectively.

The dropwise addition of undiluted or ethanol diluted titanium alkoxide into water or ethanol–water mixtures under ultrasonic irradiation was investigated [27,28]. It was reported that the application of ultrasonic irradiation facilitated the generation of the secondary phase (brookite) and increase in ethanol to water ratio induced a decrease in the peak intensities of the crystalline phases in the XRD patterns. The precipitates were amorphous when the ratio was 10.

The surface area was the largest (97 m²/g) when TIP was directly added to water while ultrasonic irradiation was applied [23]. It was reported by Mason and Lorimer (2002) that maximum ultrasound effect was obtained when the aqueous precipitation solution had a composition of 50 wt.% ethanol at 25 °C [21].

The addition of chemical species such as triblock copolymers [27], acetic acid [28] and amines [29,30] was investigated to adjust the pore/phase structure of the powders. However, an additional step, extraction by nitric acid was required to remove amines. The use of acetic acid was related with the emergence of secondary phases and the prepared powder was not crystalline at 100 °C in this investigation [28] in contrast to the observations reported in other investigations [23,26,27,30]. The effect of ultrasonic irradiation was not found as significant in terms of crystallite size and surface area. The surface equivalent particle size and surface area of pure anatase titania were 23 nm and 67 m²/g at 400 °C.

This article intends to investigate the progress of nanotitania structure prepared by ultrasonic induced hydrolysis with increasing temperature in terms of phase structure and crystallite size, surface area, pore size and particle size distribution, powder density and densification behavior. The properties of these mesoporous nanocrystalline titania powders were compared with titania powder prepared without ultrasonic treatment and Degussa P-25. The dilatometric densification curves of these powders were further determined and analyzed which may generate valuable information on the microstructure evolution upon heat treatment of these promising nanomaterials.

2. Materials and methods

2.1. Synthesis

Nanocrystalline titania powders were prepared by hydrolyzing titanium isopropoxide (TIP) in ethanol–water mixture with and without the application of ultrasonic irradiation, which were labeled as TiO_2-U and TiO_2-NoU, respectively. The schematic flowchart of the TiO_2-U powder processing is shown in Fig. 1. The TIP–ethanol mixture (1.00 mol/L) was stirred for 30 min initially. Ethanol–water mixture (1:1 by volume) was subjected to ultrasonic irradiation (Ultrasonic Cleaner, 37 kHz, Elmasonic 80S), while TIP–ethanol mixture was added dropwise by using a peristaltic pump (10 mL/min). A typical experiment was completed in 20 min and the temperature of the ultrasonic bath did not exceed 40 °C. The TiO_2-NoU powder was prepared by following the same procedure without applying ultrasonic irradiation during hydrolysis. Bluish white precipitates were formed instantaneously and recovered by centrifugation (8000 rpm for 30 min) at the end of precipitation. The precipitates were dried at 70 °C for 12 h and heat treated at different temperatures (100–800 °C) with a heating rate of 10 °C/min and a soaking time of 2 h
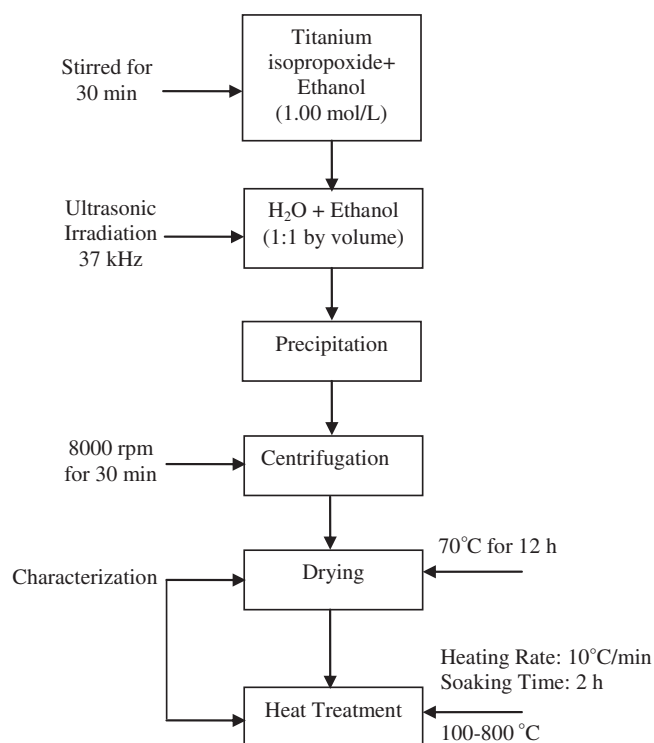

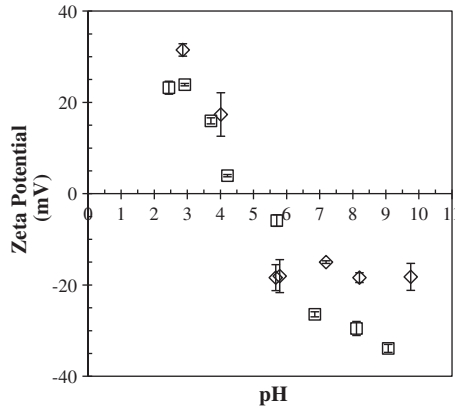Fig. 1. Flowchart of nanocrystalline titania preparation under ultrasonic irradiation.

Fig. 2. The variation of zeta potentials of nanotitania (TiO$_2$-U) heat treated at 425 °C (□) and Degussa P-25 (◊) with pH.

at the peak temperature. Degussa P-25, commercial titania powder was also characterized similarly.

2.2. Characterization methods

The particle size distributions and isoelectric (IEP) points of the powders were determined by using ZetaSizer (3000 HS$_A$, Malvern). Dilute suspensions were prepared by adding about 0.5 mg of powder into a UV cuvette in about 2–3 mL of ultrapure water. The dispersion was subjected to ultrasonic treatment for 30 min before measurement. The pH was adjusted by adding dilute nitric acid and ammonia solution for the zeta potential measurements. The IEP measurements were repeated three times and the standard deviations were indicated in the related figure. The BET surface area of the powders and the BJH desorption curves were determined by N$_2$ sorption by using Micromeritics ASAP 2000. The samples were degassed at a temperature which was 50 °C below powder heat treatment temperature. An adsorption data in the relative pressure (P/P$_o$) range of 0.05–0.3 was used to determine the surface area by BET (Brunauer–Emmett–Teller) method. Desorption data was used to determine the pore size distribution by BJH (Barret–Joyner–Halender) method by assuming a cylindrical pore model. These sorption characterizations were carried out only once on each sample since they were approximately one day long runs. He pycnometer was used to determine the density of the powders at room temperature. The density measurements

were repeated three times and the average density was calculated. The XRD patterns were obtained by Philips Expert Pro XRD using CuK$_\alpha$ radiation in the 20–60° 2θ range and only one pattern for each sample was obtained. The average crystallite size (ACS) of the powders was calculated by using Scherrer equation from the full-width half-maximum of the peak of each phase after correcting for the instrumental broadening by using the X'PERT PLUS program (version 1.0, 23.04.1999). Due to the overlap of anatase (110) peak with brookite (120) and (111) peaks, the ACS of the samples was calculated from the second strongest anatase peak (200) located at 2θ of ~48°. The ACS of rutile was calculated from the (110) peak which is located at 2θ of ~27°. Anatase, brookite, and rutile phase contents of the powders were determined by using the following equations:

$$w_A\% = \frac{100 \cdot k_A I_A}{k_A I_A + I_R + k_B I_B} \tag{1}$$

$$w_R\% = \frac{100 \cdot I_R}{k_A I_A + I_R + k_B I_B} \tag{2}$$

$$w_B\% = \frac{100 \cdot k_B I_B}{k_A I_A + I_R + k_B I_B} \tag{3}$$

where w_A, w_B, and w_R are weight percents of anatase, brookite, and rutile phases in the sample, I_A, I_B, and I_R are integrated peak intensities of the strongest anatase (101), brookite (211), and rutile (110) peaks. The coefficients k_A and k_B are obtained from previous work as 0.886 and 2.721 [26,27,31].

The TGA curves of the powders were obtained by heating to a maximum temperature of 1000 °C under N$_2$ atmosphere at a heating rate of 10 °C/min. The densification behavior of the powder compacts isostatically pressed at 210 MPa was determined by using a dilatometer (Linseis, L76/150B) with a heating rate of 5 or 10 °C/min up to 1200 °C. TGA and dilatometric measurements were conducted only once on each sample reported in this work.

3. Results and discussion

The variation of the zeta potentials of the powders with pH is shown in Fig. 2. The IEP of the nanotitania powder (TiO$_2$-U) and Degussa P-25 powder was about 5. Due to the relatively low zeta potential values which are 5.1 and −16.1 mV at pH values of 4 and 6, the TiO$_2$-U powder was considered colloidally unstable in this
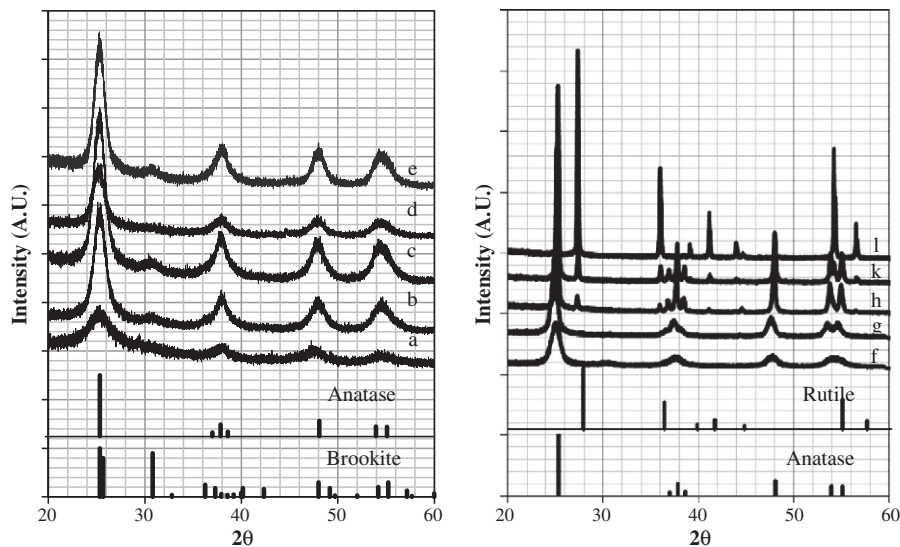

Fig. 3. The XRD patterns of TiO$_2$-NoU heat treated at (a) 25, (b) 70, (c) 100, (d) 250, (e) 300, (f) 400, (g) 500, (h) 600, (k) 700 and (l) 800 °C.
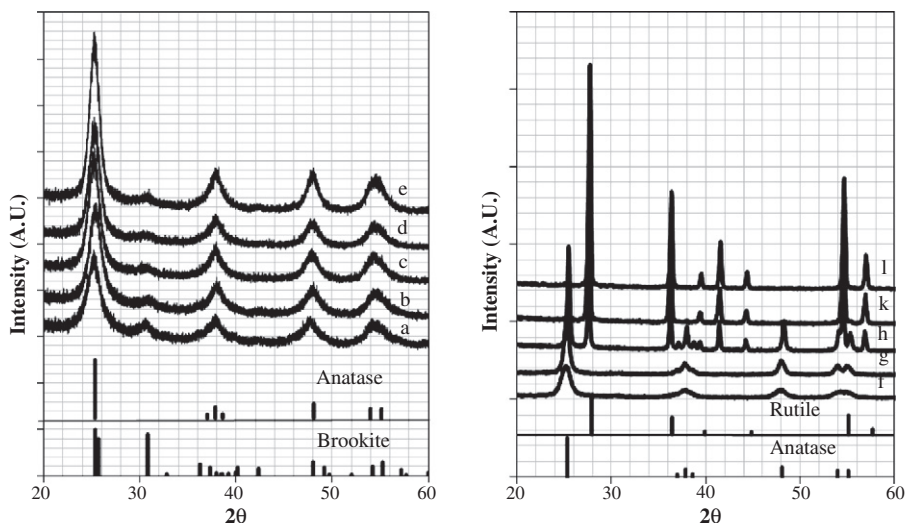
Fig. 4. The XRD patterns of TiO₂-U heat treated at (a) 25, (b) 70, (c) 150, (d) 250, (e) 300, (f) 400, (g) 500, (h) 600, (k) 700 and (l) 800 °C.

range. Higher zeta potentials as 23 and − 30 mV at pH levels of 2.9 and 8.1 were determined.

The effects of ultrasonic irradiation and heat treatment temperature on the ACS and phase contents of the powders were determined from their XRD patterns based on the standard XRD patterns of anatase, brookite, and rutile phases (JCPDS 84-1286, 29-1360, and 88-1175, respectively). Although only broad anatase peaks were detected in the XRD pattern of TiO₂-NoU-25, the brookite peak (~30.8° of 2θ) became detectable in the 70–400 °C range (Fig. 3). The rutile phase formation started at above 500 °C and was completed at ~800 °C. The brookite and anatase peaks became sharper in the ultrasonically treated powders compared to their counter parts in the untreated powders as can be seen in Figs. 3 and 4. The brookite phase completely transformed into anatase in the 400–500 °C temperature range. The anatase to rutile phase transformation started at lower than 600 °C and was completed at temperatures in between 700 and 800 °C range for TiO₂-U.

The weight percentages of the crystalline phases were determined as outlined previously and further plotted as a function of temperature in Fig. 5. The TiO₂-NoU powder consists of only anatase phase (~100 wt.%) in the room temperature to 70 °C range. The brookite phase (10–13 wt.%) which forms at ~70 °C, completely transformed to anatase in the 400–500 °C range. It was observed that the application of ultrasonic irradiation favors the formation of the brookite phase (60 wt.% of anatase and 40 wt.% of brookite for TiO₂-U-25).

However, the amount of the brookite phase decreased to 25 wt.% at 70 °C. The TiO₂-U powder contained 9 wt.% brookite phase at 400 °C and pure anatase was obtained by heating to 500 °C. The anatase to rutile phase transformation occurred above 500 °C and was completed at 800 °C for both powders.

Particle coarsening in the powders during phase transformation was detected via analyzing the increase in the ACS of the anatase phase determined by using Scherrer equation and surface area equivalent particle size (SAEPS) (Fig. 6). The ACS of TiO₂-NoU-25 which was two times larger than the TiO₂-U-25, did not change significantly (~10 nm) in the 70–400 °C range. It increased significantly in the 500–800 °C temperature range where also anatase–rutile transformation occurred. The increases in ACS for TiO₂-U powder were observed to occur at two separate temperature ranges of 25–200 and 400–600 °C. The ACS of TiO₂-U powder was almost constant during phase transformations at temperatures of 250–400 °C (brookite to anatase) and 600–700 °C (anatase to rutile). A significant increase in crystallite size was observed in the 400–800 °C range for both powders. The SAEPS was calculated from BET surface areas by assuming that the particles are non-porous spherical particles and was quite comparable with the XRD data driven ACS in the 200–500 °C range as seen in Fig. 5. The crystallite size of Degussa P-25 powder was calculated as 17 nm based on the strongest (110) anatase peak).

The N₂ adsorption–desorption isotherms of both TiO₂-U and TiO₂-NoU powders heat treated at different temperatures (200–500 °C)

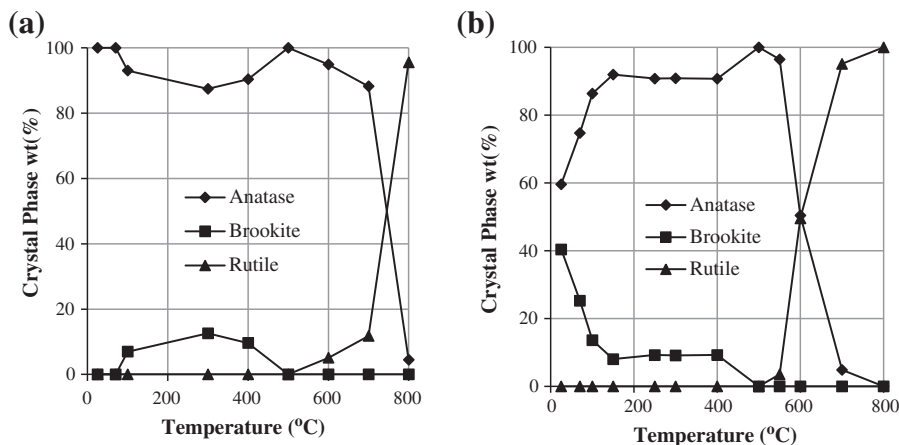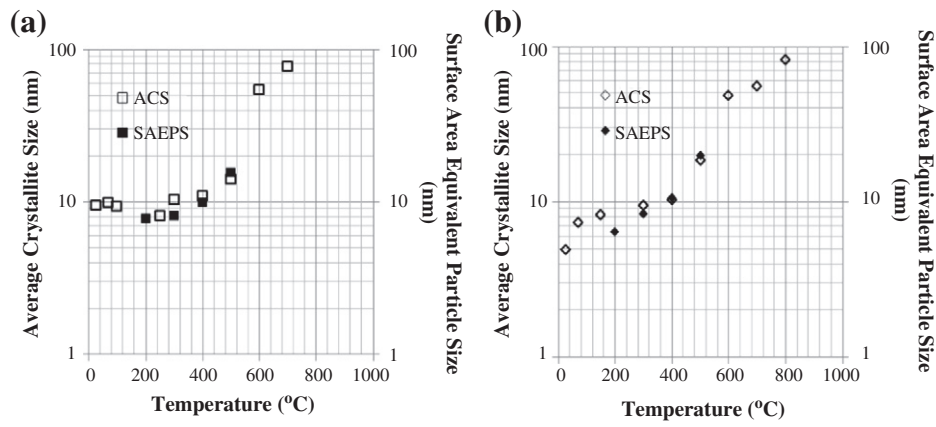**Fig. 5.** The variation of the wt.% of the crystalline phases present in (a) TiO2-NoU and (b) TiO2-U powders with respect to temperature.

Fig. 6. The effect of temperature on average crystal size (ACS) and surface equivalent particle size (SAEPS) of (a) TiO$_2$-NoU and of (b) TiO$_2$-U powders.

exhibit type IV isotherms with H3 hysteresis loops [32,33]. The locations and the forms of the hysteresis loops indicated high adsorption energy and mesoporous structure with slit shaped pores in the range of 2–50 nm (Figs. 7 and 8) according to BDDT (Brunauer, Deming, Deming and Teller) classification. However, the Degussa P-25 powder had type II adsorption isotherm which is characteristic of non-porous or macroporous structures with high adsorption energy (Fig. 9).

The hysteresis loop of TiO$_2$-NoU-200 was located in the relative pressure range of 0.5–1 and gradually shifted to 0.6–1 relative pressure range when it was heat treated at 400 °C. The pore volumes of TiO$_2$-NoU powders (~0.36 m^3/g) did not change significantly, but broader pore size distributions and a monotonic decrease in the BET surface areas were determined by increasing the heat treatment temperature up to 400 °C (Table 1 and Fig. 10a). The average pore size
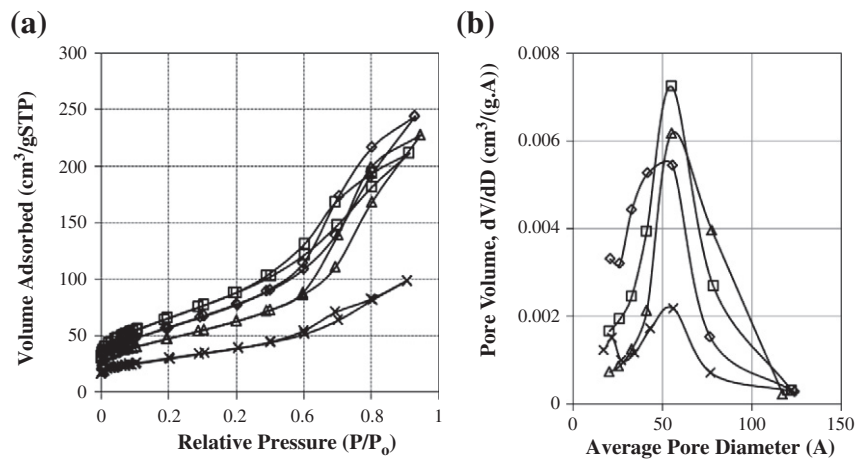

Fig. 7. (a) The N$_2$-sorption isotherms and (b) BJH desorption pore size distributions of TiO$_2$-NoU titania powders heated at 200 (□), 300 (◊), 400 (△), and 500 °C (×).

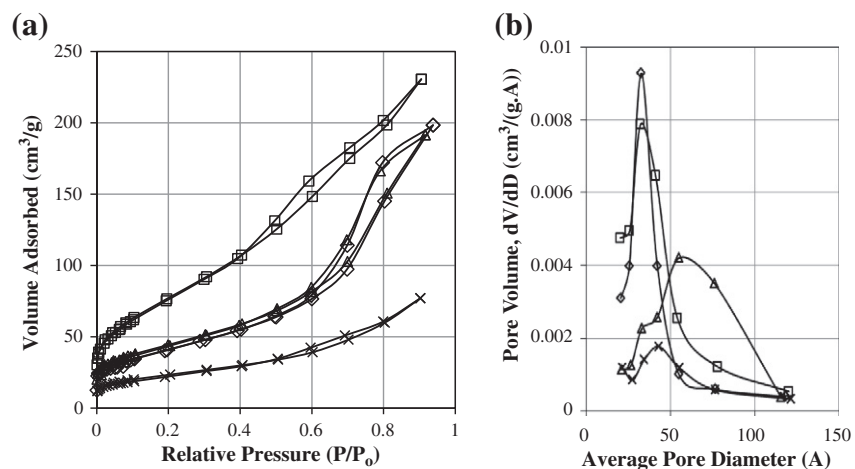**Fig. 8.** (a) The N$_2$-sorption isotherms and (b) BJH desorption pore size distributions of TiO$_2$-U titania powders heated at 200 (□), 300 (◊), 400 (△),and 500 °C (×).
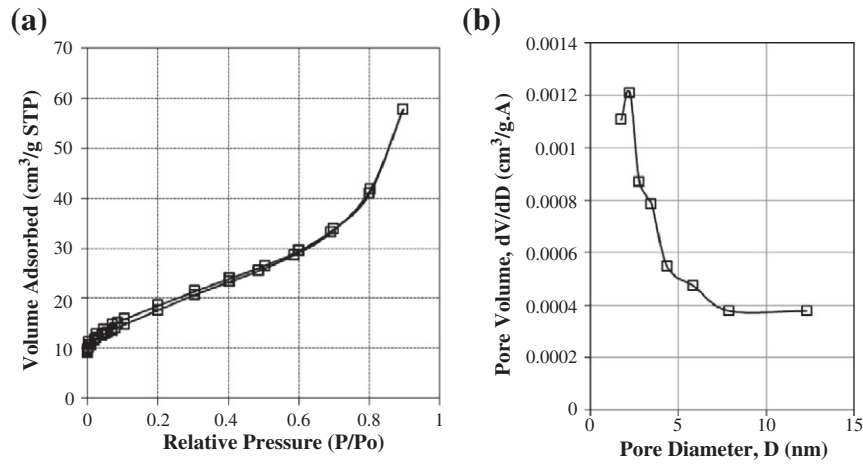
Fig. 9. (a) The N_2-sorption isotherms and (b) BJH desorption pore size distribution of Degussa P-25 (□).

Table 1
The pore/phase structure properties, surface areas and He pycnometer densities of the powders.

Sample	Average crystallite size (nm)	Anatase content (%w_A)	Brookite content (%w_B)	Rutile content (%w_R)	Density (g/cm^3)	BET (m^2/g)	Average pore size[a] (nm)	Pore volume[a] (cm^3/g)
TiO$_2$-NoU-25	9.9	100	–	–	–	–	–	–
TiO$_2$-NoU-70	9.7	100	–	–	–	–	–	–
TiO$_2$-NoU-100	9.3	97	3	–	–	–	–	–
TiO$_2$-NoU-200	–	–	–	–	–	238	5.5	0.327
TiO$_2$-NoU-300	10.2	87	13	–	–	209	7.2	0.378
TiO$_2$-NoU-400	10.9	90	10	–	–	170	8.2	0.352
TiO$_2$-NoU-500	14	100	–	–	–	106	5.7	0.153
TiO$_2$-NoU-600	54	95	–	5	–	–	–	–
TiO$_2$-NoU-700	78	88	–	12	–	–	–	–
TiO$_2$-NoU-800	292[b]	4	–	96	–	–	–	–
TiO$_2$-U-25	4.9	60	40	–	–	–	–	–
TiO$_2$-U-70	7.3	75	25	–	3.19	–	–	–
TiO$_2$-U-150	8.2	92	8	–	–	–	–	–
TiO$_2$-U-100	8	86	14	–	–	–	–	–
TiO$_2$-U-200	–	–	–	–	3.27	287	4.2	0.336
TiO$_2$-U-250	8.1	91	9	–	–	–	–	–
TiO$_2$-U-300	9.4	91	9	–	3.57	201	4	0.246
TiO$_2$-U-400	10.3	91	9	–	3.57	159	5.9	0.297
TiO$_2$-U-500	18.4	100	–	0	3.68	82	5.4	0.117
TiO$_2$-U-600	48	50	–	50	4.06	–	–	–
TiO$_2$-U-700	55[b]	5	–	95	4.00	–	–	–
TiO$_2$-U-800	81[b]	–	–	100	4.13	–	–	–
Degussa P-25	17	13	–	97	–	66	5	0.09

[a] From BJH desorption data.
[b] Calculated from X-ray peak of rutile located at 27.2° of 2θ.

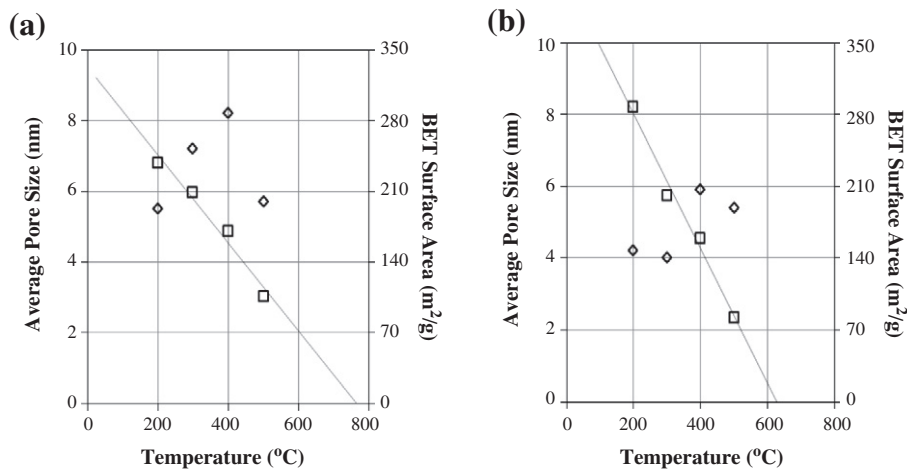**Fig. 10.** The variation of BET surface area (□) and pore size based on BJH desorption (◇) with temperature of (a) TiO$_2$-NoU and (b) TiO$_2$-U powders.
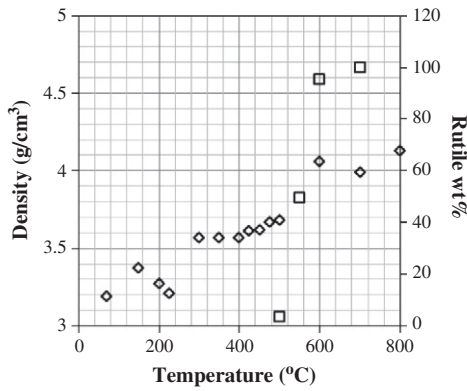
Fig. 11. The variation of density of nanotitania ($\diamond$) and w_R, % rutile, ($\square$) with respect to temperature for TiO_2-U.

The variation of the hysteresis loop form and location for TiO_2-U powder with temperature have shown a two-step progress: the shift to a higher relative pressure range ($P/P_o \sim 0.4$–1 to 0.5–1) by increasing calcination temperature from 200 to 300/400 °C and a further narrowing of the relative pressure range ($P/P_o \sim 0.5$–1 to 0.5–0.8) at 500 °C (Fig. 8). Similarly, the pore size distribution became narrower by heating up to 300 °C and became wider by further heat treatment. The BET surface area (from 287 to 80 m^2/g) and the BJH pore volume (from 0.334 to 0.117 cm^3/g) decreased significantly by increasing the heat treatment temperature from 200 to 500 °C whereas the average pore size didn't change significantly (~4–5.4 nm) for TiO_2-U powder (Table 1 and Fig. 10b). The first step may be dominated by the formation of anatase phase and crystal growth which eliminated inter-particle pores in the 200-400 °C range. The second step may be related to the reduction of smaller pores preferentially and the presence of larger pores due to the formation of closely packed aggregates while heating from 400 to 500 °C [34,35].

The pore/phase structure properties, surface areas and He pycnometer densities of the powders are further tabulated in Table 1. The variation of the powder densities with heat treatment temperature is given in Fig. 11. The densities of the powders were determined to be above 4.00 g/cm^3 for heat treatment temperatures above 600 °C which became comparable with the density of rutile in agreement with the XRD results. The powder density is almost constant in the 300–500 °C range (in the 3.57–3.68 g/cm^3) which is close to the
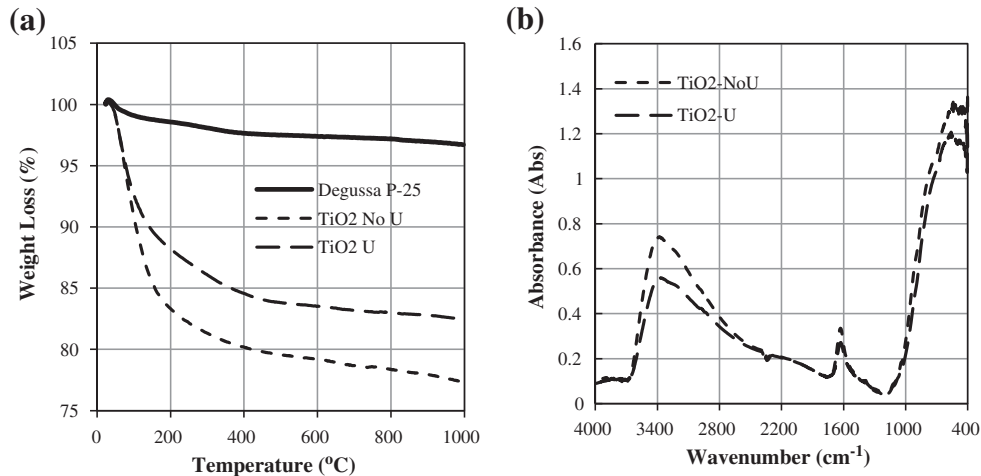
became larger (5.5 to 8.2 nm) in the 200–400 °C range due to the formation of larger aggregates while the BJH pore volume did not change significantly (0.327 to 0.357 cm^3/g) for TiO_2-NoU powder. The average pore size, pore volume and surface area decreased to 5.7 nm, 0.153 cm^3/g and 106 m^2/g, respectively, at 500 °C due to the formation of densely packed aggregates.

Fig. 12. (a) TGA curves of Degussa P-25, TiO_2-NoU and TiO_2-U under N2 atmosphere (b) FTIR curves of TiO_2-NoU and TiO_2-U powders which were dried at 25 °C.
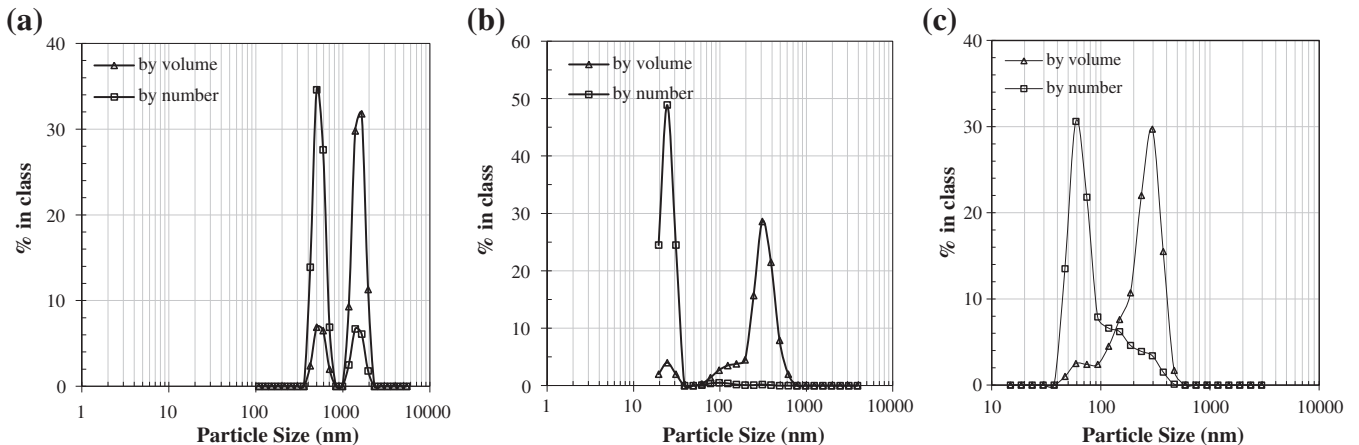

Fig. 13. The particle size distribution of (a) TiO_2-U as precipitated, (b) TiO_2-U-425, and (c) Degussa P-25 by DLS measurement.

Table 2
The average particle size of TiO$_2$-U and Degussa P-25 by volume and by number.

Sample	Particle size by volume (nm)	Particle size by number (nm)	Polydispersity index	SAEPS (nm)
TiO$_2$-U as precipitated	545 (18%) 1536 (82%)	549 (83%) 1545 (17%)	0.062	–
TiO$_2$-U-425	25 (8%) 309 (92%)	25 (98%) 109 (2%)	0.475	9.7
Degussa P-25	72 (8%) 259 (92%)	98 (100%)	–	22

anatase phase density. The density increases with heat treatment temperature initially with a subsequent decrease in the 70–225 °C range which may be attributed to the brookite phase transformation to anatase and the rearrangements in the amorphous phase present in the powders. The powder density was 4.13 g/cm^3 at 800 °C after the completion of anatase to rutile phase transformation (in the 500–800 °C range).

The TGA curve of the titania powders (dried at room temperature) and Degussa P-25 are given in Fig. 12a. Degussa P-25 powder lost about 3 wt.% of its original weight in the 25–1000 °C range, which was attributed to the removal of physically adsorbed water from powder surface. Total weight loss of TiO$_2$-NoU and TiO$_2$-U powders up to 1000 °C was 23 and 17.5 wt.%, respectively. The weight loss in the 25–80 °C range was about 5 wt.% for both titania powders which was attributed to the removal of physically/chemically adsorbed water and ethanol. The weight loss of TiO$_2$-NoU was about 5 wt.% higher than TiO$_2$-U powder with further heating to 200 °C and this behavior may be related to the presence of Ti(OH)$_4$ and its transformation to TiO$_2$ upon further heating which was confirmed by FTIR spectrum (Fig. 12b). The broad peak located at 3340 cm^{-1} indicated the presence of surface hydroxyls (Ti(OH)$_4$). The adsorbed water was detected by the peak located at 1620 cm^{-1}. The intensities of the defined peaks for TiO$_2$-NoU were higher than TiO$_2$-U which was consistent with the presence of a higher level of Ti(OH)$_4$ in TiO$_2$-NoU.

The particle size distributions and the average particle sizes of TiO$_2$-U and Degussa P-25 powders are given in Fig. 13 and Table 2. The particle size of Degussa P-25 by dynamic light scattering (DLS) was almost five times higher than the SAEPS. Although DLS operates on the assumption of the presence of homogenous and non-absorbing spherical particles in dilute suspensions, this assumption may be violated due to non-spherical shape and porous powders. The as-precipitated particles (TiO$_2$-U) were partially crystalline and contained hydroxyl groups, chemically adsorbed water and ethanol based on the findings of XRD, TGA and FTIR analyses. They may

have larger surface area than TiO$_2$-U-200 (287 m^2/g) and were largely agglomerated. The most of TiO$_2$-U as precipitated particles was about 550 nm (83% of particles) in size by number. The particle size of TiO$_2$-U-425 (146 m^2/g) was about 25 nm (97.8 and 2.2% of nanoparticles were 25 and 109 nm in size by number, respectively) due to the removal of adsorbed chemicals and progress of crystalline phases during heat treatment.

The polydispersity index (PDI) values of the measurements are given in Table 2. The PDI value is related with the dispersivity and varies between 0 and 1. The more monodisperse the particles are, the lower the PDI value. TiO$_2$-U as precipitated powder contained 500 nm and 1.5 μm particles in size which correspond to amorphous aggregates formed in the precipitation medium and their larger agglomerates. The PDI value of particle size measurement for TiO$_2$-U-425 powder was 0.475 which represents a broader particle size distribution. This may be due to the formation of a relatively large amount of smaller particles (25 nm in size which is closer to the 10 nm crystallite size) during the removal of hydroxyl groups and the formation of crystalline phases and aggregates upon heat treatment.

The powder compacts had a densification behavior which was formed of two stages, which are given in Fig. 14a and b. There was no significant shrinkage (~2%) present in TiO$_2$-NoU and TiO$_2$-U powder compacts up to 200 °C and 400 °C for Degussa P-25 powder compacts regardless of heating rate. The first stage in the 500–850 °C range may most likely be controlled by the 7–10 nm crystallites in the structure and account for 18% of the total 26% shrinkage at 1200 °C with a heating rate of 10 °C/min. The second stage starting from 850 °C may be due to the sintering of densified submicron original aggregates of the powder primary crystallites. The densification of TiO$_2$-NoU and TiO$_2$-U powders still was not completed by 1200 °C.

The progress of microstructure development, sintering stages, and phase transformations of the powder compacts with respect to temperature can be differentiated by evaluation of the first derivatives of the shrinkage curves (Fig. 15a and b). The peak temperatures were ~30 °C higher upon increasing the heating rate from 5 to 10 °C/min. There was no shrinkage at temperatures up to 400 °C for powder compacts of Degussa P-25compacts. Increasing the heating rate from 5 to 10 °C/min lowers the peak temperatures of sintering stages for anatase (C) and rutile (E) as seen Fig. 15a and b. The TiO$_2$-NoU powder compacts had a slightly higher total shrinkage at 1200 °C although the peak densification temperatures were the same. The removal of hydroxides was observed at 200 °C for TiO$_2$-NoU and TiO$_2$-U while brookite to anatase phase transformation was in progress (A). The phase transformation of brookite to anatase was not detected from the first derivatives of the shrinkage curves in the 300–500 °C range (B) due to the low content of brookite (13 and
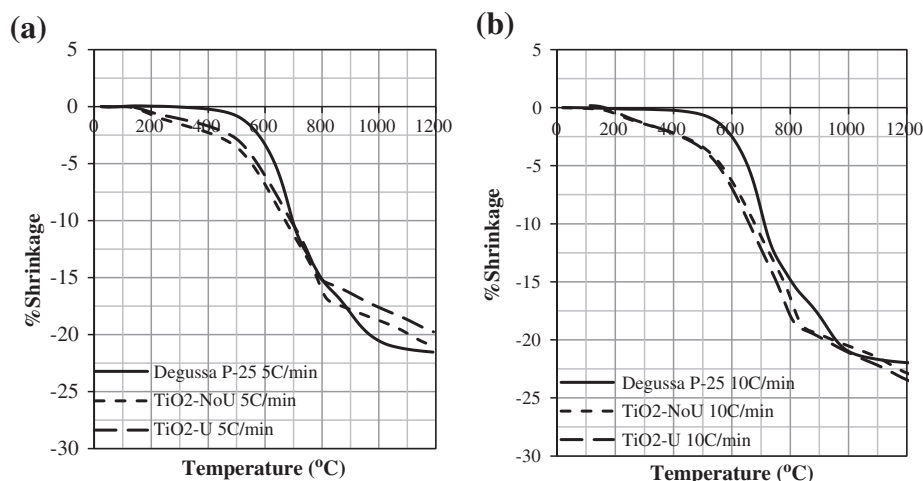

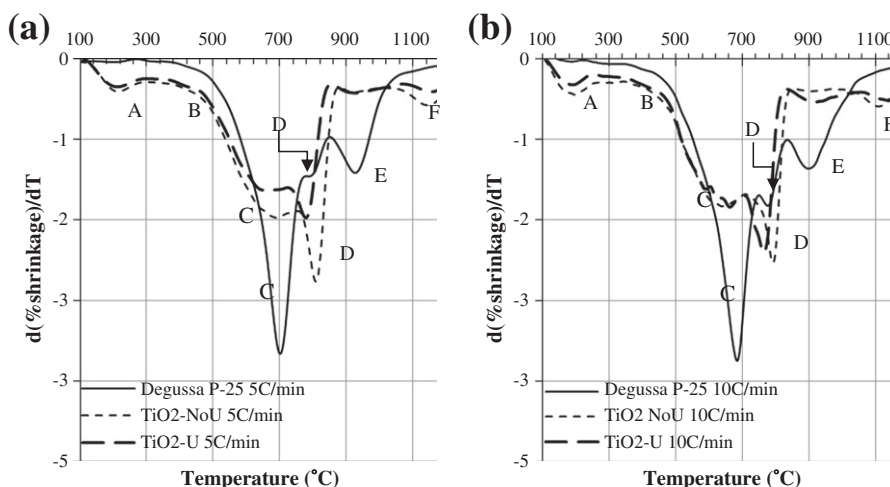**Fig. 14.** The shrinkage curves of Degussa P-25, TiO$_2$-NoU and TiO$_2$-U at a heating rate of (a) 5 °C/min and (b) 10 °C/min.

Fig. 15. The first derivative of the shrinkage curves of Degussa P-25, TiO$_2$-NoU and TiO$_2$-U at a heating rate of (a) 5 °C/min and (b) 10 °C/min. (A: the removal of hydroxides; B: the phase transformation of brookite to anatase; C: the sintering of anatase; D: the phase transformation of anatase to rutile; E: the sintering of rutile and aggregates, F: further sintering due to the formation of pores between submicron sized densified aggregates).

9 wt.% for TiO$_2$-NoU and TiO$_2$-U, respectively). The intense and significantly broad peak observed for Degussa P-25 located at 650–700 °C was attributed to the sintering of anatase (C). The rate of anatase to rutile phase transformation for Degussa P-25 with ~13 wt.% rutile, was not as significant as for both TiO$_2$-NoU and TiO$_2$-U powder compacts (D). The peaks located at 900 °C for Degussa P-25, TiO$_2$-NoU and TiO$_2$-U were attributed to the sintering of rutile phase and submicron sized densified aggregates (E). The shrinkage of TiO$_2$-NoU and TiO$_2$-U powder compacts was still in progress above 1000 °C which was attributed to further sintering due to the formation of pores between submicron sized densified aggregates (F).

4. Conclusions

Nanocrystalline titania powders were prepared by hydrolysis of titanium isopropoxide with or without ultrasonic irradiation at room temperature. The application of ultrasonic irradiation during hydrolysis favors the formation of brookite phase, smaller crystallites, higher surface area/pore volume, and narrower pore size distribution. Pure anatase phase was obtained after heat treatment at 500 °C. The anatase to rutile phase transformation started in the 500–550 °C range and was completed at 800 °C for both TiO$_2$-NoU and TiO$_2$-U powders. The TiO$_2$-NoU and TiO$_2$-U powders displayed mesoporous structure and indicated the presence of slit shaped pores with high adsorption energy. Commercial Degussa P-25 powder on the other hand was determined to have a macroporous structure. The pore size distribution became wider and the pore volume was reduced by heat treatment which may be related to the collapse of small pores and the formation of larger crystallites hence a coarser pore structure. The presence of Ti(OH)$_4$ was confirmed by FTIR analyses and its transformation to TiO$_2$ upon heating to 200 °C was detected by TGA analyses. The TGA total weight loss of TiO$_2$-NoU was about 5 wt.% higher than TiO$_2$-U powder. The DLS particle size analysis revealed the presence of 25 and 109 nm nanoparticles (about 97.8 and 2.2% by number respectively) in the TiO$_2$-U-425 powder. The dilatometric shrinkage curve of nanotitania has shown a two stage sintering behavior where the former stage may be controlled by small crystallites (7–10 nm) in the 500–850 °C range and the latter by aggregates with sizes in submicron range. The phase structure evolution in the powder compacts during sintering was analyzed by the first derivatives of the shrinkage curves which may prove to be very useful for titania based nano material characterization.

References

[1] M.J. Mayo, M. Ciftcioglu, Issues in the processing of bulk nanocrystalline ceramics for structural applications, in: cluster and cluster assembled materials, in: R.S. Averback, P.L. Nelson, J. Bernhole (Eds.), MRS SYmp. Proc., 206, Materials Research Society, Pittsburg, USA, 1991, pp. 545–550.
[2] G.S. Devi, T. Hyodo, Y. Shimizu, M. Egashira, Nanostructured titania (TiO$_2$) as hydrogen gas sensor Proc, SPIE 5062 (2003) 106–110.
[3] S.A. Akbar, L.B. Younkman, Ceramic based resistive sensors, Journal of the Electrochemical Society 144 (1997) 1750–1753.
[4] A. Fujishima, K. Honda, Electrochemical photolysis of water at a semiconductor electrode, Nature 238 (1972) 37–38.
[5] K. Hashimoto, H. Irie, A. Fujishima, TiO$_2$ photocatalysis: a historical overview and future prospects, Japanese Journal of Applied Physics 44 (2005) 8269–8285.
[6] F. Han, V.S.R. Kambala, M. Srinivasan, D. Rajarathnam, R. Naidu, Tailored titanium dioxide photocatalysts for the degradation of organic dyes in wastewater treatment: a review, Applied Catalysis A: General 359 (2009) 25–40.
[7] C.A. Countinho, V.K. Gupta, Photocatalytic degradation of methyl orange using polymer–titania microcomposites, Journal of Colloid and Interface Science 333 (2009) 457–464.
[8] D.M. Blake, P.-C. Maness, Z. Huang, E.J. Wolfrum, J. Huang, W.A. Jacoby, Application of the photocatalytic chemistry of titanium dioxide to disinfection and the killing of cancer cells, Separation and Purification Reviews 28 (1999) 1–50.
[9] K.-S. Lin, H.-W. Cheng, W.-R. Chen, C.-H. Wu, Synthesis, characterization, and adsorption kinetics of titania nanotubes for basic dye wastewater treatment, Adsorption 16 (2010) 47–56.
[10] J. Blanco-Galvez, P. Fernandez-Ibanez, S. Malato-Rodrigez, Solar photocatalytic detoxification and disinfection of water: recent overview, Transactions of the ASME 129 (2007) 4–15.
[11] M.F. Dadjour, C. Ogino, S. Matsumura, N. Shimuzu, Kinetics of disinfection of *Escherichia coli* by catalytic ultrasonic irradiation with TiO$_2$, Biochemical Engineering Journal 25 (2005) 243–248.
[12] J. Zhu, M. Zach, Nanostructured materials for photocatalytic hydrogen production, Current Opinion in Colloid & Interface Science 14 (2009) 260–269.
[13] D. Gust, D. Kramer, A. Moore, T.A. Moore, W. Vermaas, Engineered and artificial photosynthesis: human ingenuity enters the game, MRS Bulletin 33 (2008) 383–387.
[14] K. Kalyanasundaram, M. Graetzel, Artificial photosynthesis: biomimetic approaches to solar energy conversion and storage, Current Opinion in Biotechnology 21 (2010) 298–310.
[15] M. Faustini, L. Nicole, C. Boissiere, P. Innocenzi, C. Sanchez, D. Grosso, Hydrophobic, antireflective, self-cleaning, and antifogging sol–gel coatings: an example of multifunctional nanostructured materials for photovoltaic cells, Chemistry of Materials 22 (2010) 4406–4413.
[16] X. Chen, S.S. Mao, Titaniumdioxide nanomaterials: synthesis, properties, modifications and applications, Chemical Reviews 107 (2007) 2891–2959.
[17] K. Suslick, Kirk-Othmer Encyclopedia of Chemical Technology, fourth ed. John Wiley and Sons, Inc., New York, 1998.
[18] K. Suslick, G.J. Price, Applications of ultrasound to materials chemistry, Annual Review of Materials Science 29 (1999) 295–326.
[19] Gedanken, Sonochemistry and its application to nanochemistry, Current Science 85 (2003) 1720–1722.
[20] Gedanken, Using sonochemistry for the fabrication of nanomaterials, Sonochemistry 11 (2004) 47–55.
[21] T.J. Mason, J.P. Lorimer, Applied Sonochemistry, Wiley-VCH Verlag GmbH & Co. KGaA, Weinheim, 2002.

Ö.Ç. Duvarci, M. Çiftçioğlu / Powder Technology 228 (2012) 231–240

[22] S.-Y. Kim, T.-S. Chang, C.-H. Shin, Enhancing effects of ultrasound treatment on the preparation of TiO2 photocatalysts, Catalysis Letters 118 (2007) 224–230.

[23] J.C. Yu, J. Yu, W. Ho, L. Zhang, Preparation of highly photocatalytic active nano-sized TiO2 particles via ultrasonic irradiation, Chemical Communications (2001) 1942–1943.

[24] C.W. Oh, G.-D. Lee, S.S. Park, C.-S. Ju, S.-S. Hong, Preparation of nanosized TiO$_2$ particles via ultrasonic irradiation and their photocatalytic activity on the decomposition of 4-nitrophenol, Korean Journal of Chemical Engineering 22 (2005) 547–551.

[25] W. Huang, X. Tang, Y. Wang, Y. Koltypin, A. Gedaken, Selective synthesis of anatase and rutile via ultrasound irradiation, Chemical Communications 12 (2000) 1183–1186.

[26] J. Yu, M. Zhou, C. Cheng, H. Yu, X. Zhao, Ultrasonic preparation of mesoporous titanium dioxide nanocrystalline photocatalysts and evaluation of photocatalytic activity, Journal of Molecular Catalysis A: Chemical 227 (2005) 75–80.

[27] J.C. Yu, L. Zhang, J. Yu, Direct sonochemical preparation and characterization of highly active mesoporous TiO2 with a bicrystalline framework, Chemistry of Materials 14 (2002) 4647–4653.

[28] P.S. Awati, S.V. Awate, P.P. Shah, V. Ramaswamy, Photocatalytic decomposition of methylene blue using nanocrystalline anatase titania prepared by ultrasonic technique, Catalysis Communications 4 (2003) 393–400.

[29] Y. Wang, X. Tang, W. Huang, Y.R. Hacohen, A. Gedaken, Sonochemical synthesis of mesoporous titanium oxide withwormhole-like framework structures, Advanced Materials 16 (2000) 1183–1186.

[30] Y.-Q. Wang, S.-G. Chen, Z.-H. Tang, O. Palchik, A. Zaban, Y. Koltypin, A. Gedanken, Mesoporous titanium dioxide: sonochemical synthesis and application in dye-sensitized solar cells, Journal of Materials Chemistry 11 (2001) 521–526.

[31] H. Zhang, J.F. Banfield, Understanding polymorphic phase transformation behavior during growth of nanocrystalline aggregates: insights from TiO$_2$, The Journal of Physical Chemistry. B 104 (2000) 3481.

[32] J.B. Condon, Surface Area and Porosity Determinations by Physisorption, Elsevier Publications, Amsterdam, 2006.

[33] F. Rouquerol, J. Rouquerol, K. Sing, Adsorption by Powders and Porous Solids, Academic Press, San Diego, 1999.

[34] J. Yu, S. Liu, H. Yu, Microstructure and photoactivity of mesoporous anatase hollow microspheres fabricated by flüoride-mediated self-transformation, Journal of Catalysis 249 (2007) 59–66.

[35] J. Yu, J.C. Yu, M.K.-P. Leung, W. Ho, B. Cheng, X. Zhao, J. Zhao, Effects of acidic and basic hydrolysis catalysts on the photocatalytic activity and microstructures of bimodal mesoporous titania, Journal of Catalysis 217 (2003) 69–78.